

See discussions, stats, and author profiles for this publication at: <https://www.researchgate.net/publication/43132941>

A New Amorphous Semiconducting Polythiophene for High-Performance Organic Thin-Film Transistors

ARTICLE in ACS APPLIED MATERIALS & INTERFACES · APRIL 2010

Impact Factor: 6.72 · DOI: 10.1021/am9008852 · Source: PubMed

CITATIONS

10

READS

48

10 AUTHORS, INCLUDING:



soon-ki Kwon

Gyeongsang National University

243 PUBLICATIONS 4,896 CITATIONS

[SEE PROFILE](#)



Yoon Sup Lee

Korea Advanced Institute of Science and T...

212 PUBLICATIONS 4,477 CITATIONS

[SEE PROFILE](#)

A New Amorphous Semiconducting Polythiophene for High-Performance Organic Thin-Film Transistors

Hoyoul Kong,[†] Dong Hoon Lee,[†] Jung-In Seo,[†] Ji-Young Oh,[†] Dae Sung Chung,[†] Jong-Won Park,[§] Soon-Ki Kwon,[§] Yoon Sup Lee,[†] Chan Eon Park,^{*,†} and Hong-Ku Shim^{*,†}

Department of Chemistry, Korea Advanced Institute of Science and Technology (KAIST), 373-1 Guseong-Dong, Yuseong-Gu, Daejeon 305-701, Korea, Polymer Research Institute, Department of Chemical Engineering, Pohang University of Science and Technology, Pohang, Korea, and School of Nano & Advanced Materials and Engineering Research Institute, Gyeongsang National University, Jinju, Korea

ABSTRACT A new amorphous semiconducting polymer containing dodecylthiophene rings and a rigid thieno[3,2-*b*]thiophene ring, poly(2,5-bis(3'-dodecyl-2,2'-bithiophen-5-yl)thieno[3,2-*b*]thiophene) (**NAP**), was synthesized via a microwave-assisted Stille coupling reaction. The presence of the flexible unsubstituted thiophene ring units next to the rigid fused thiophene ring caused **NAP** to have an amorphous structure. This structure was confirmed by XRD, AFM, and computational calculations. In particular, the out-of-plane XRD patterns of **NAP** thin films exhibited no reflection peaks before or after the annealing process, indicating that the films had amorphous microstructures. In addition, AFM images of the **NAP** thin films showed amorphous surface morphologies with very small root-mean-square (rms) surface roughnesses of 0.3–0.5 nm, independent of surface treatment or heat treatment. Computational calculations performed to investigate the preferred conformation of the polymer confirmed the amorphous characteristics of the **NAP** structure. On the basis of these findings, we propose how an amorphous **NAP** semiconductor can maintain high carrier mobility. A **NAP**-based TFT device exhibited a very high carrier mobility of $0.02 \text{ cm}^2 \text{ V}^{-1} \text{ s}^{-1}$ with an on/off ratio of 1×10^5 and a very small threshold voltage of -2.0 V . This carrier mobility is the highest yet reported for TFTs based on amorphous semiconductors. Thus, the present findings suggest that an amorphous semiconductor layer comprised of **NAP** would be suitable for use in high-performance organic TFTs fabricated via simple processes in which neither surface treatment nor heat treatment is necessary.

KEYWORDS: organic thin-film transistors • amorphous semiconductor • polythiophene • carrier mobility

INTRODUCTION

Organic thin-film transistors (OTFTs) based on semiconducting polymers have been the focus of much research activity as a promising alternative to conventional amorphous silicon thin-film transistors (TFTs) for low-cost electronic applications such as memory devices, smart cards, and driving circuits of large-area display devices. OTFTs have various advantageous characteristics, including solution processing (spin-coating, drop-casting, and inkjet-printing), compatibility with plastic substrates, structural flexibility, and electronic and optical tunability (1).

In general, semiconducting polymers with extended planar π -conjugated and interdigitated intermolecular ordering exhibit high charge carrier mobilities without charge traps in grain boundaries (1f, 2). Thus, semicrystalline polymers such as poly(3,3'''-didodecylquaterthiophene) (PQT-12) and poly(2,5-bis(3-alkylthiophene-2-yl)thieno[3,2-*b*]thiophene) (PBTTT) have been employed as semiconductors

with high intrinsic mobilities in OTFTs (3). However, the TFT mobilities of these semicrystalline polymers are often very strongly affected by the degree to which the structure is polycrystalline. Thus, to obtain a high mobility, it is necessary to use polymer backbone and side-chain alignment procedures such as mechanical rubbing and thermal annealing (4).

For these reasons, amorphous semiconducting materials have recently received attention. Amorphous semiconducting materials have some merits compared with semicrystalline materials for the commercialization of OTFTs. Most importantly, morphological effects are not a major consideration, which is very advantageous for OTFT fabrication (5). Specifically, TFT devices can be fabricated using amorphous semiconducting materials via simple processes that do not require annealing or surface treatments such as the inclusion of a self-assembled layer on the silicon wafer.

Veres and co-workers fabricated TFTs in which the semiconducting layers were amorphous poly(triarylamine)s (PTAAs) with mobilities on the order of $10^{-2} \text{ cm}^2 \text{ V}^{-1} \text{ s}^{-1}$ (6). Recently, our group reported an air-stable amorphous semiconducting polymer, poly[(1,2-bis-(2'-thienyl)vinyl-5',5''diyl)-alt-(9,9-diptylfluorene-2,7-diyl)] (PTVTF), with a carrier mobility of $0.02 \text{ cm}^2 \text{ V}^{-1} \text{ s}^{-1}$ (4). Although several amorphous polymers have been synthesized for other applications, only a few such polymers showing good TFT

* Corresponding author. E-mail: hkshim@kaist.ac.kr (H.-K.S.); cep@postech.ac.kr (C.E.P.). Tel: +82-42-350-2827 (H.-K.S.); +82-54-279-2269 (C.E.P.). Fax: +82-42-350-2810 (H.-K.S.); +82-54-279-8298 (C.E.P.).

Received for review December 14, 2009 and accepted March 31, 2010

[†] Korea Advanced Institute of Science and Technology.

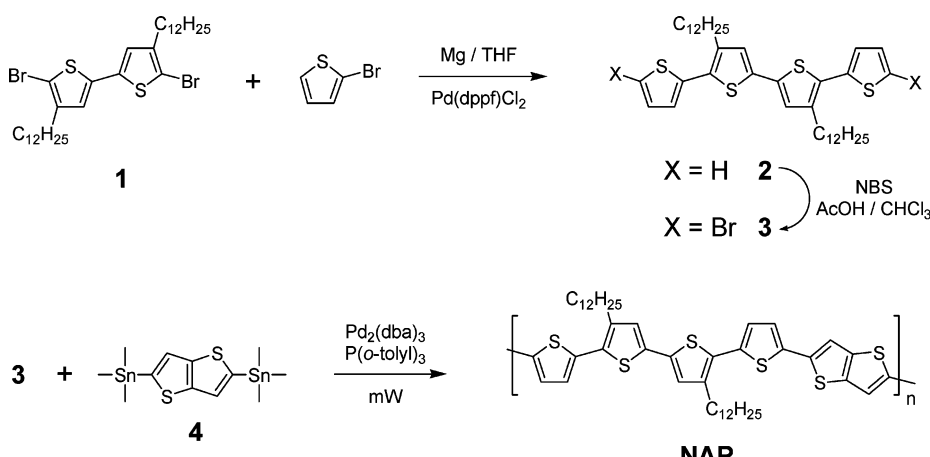
[‡] Pohang University of Science and Technology.

[§] Gyeongsang National University.

DOI: 10.1021/am9008852

2010 American Chemical Society

Scheme 1. Synthetic Route for NAP



performance have been reported because of the difficulty of controlling the relationship between structural design and TFT performance. However, some groups have sought to delineate the relation between the structures of molecules that form amorphous materials and the electronic performance of such materials. For example, McCullough's group reported a highly disordered semiconducting polymer with a very high TFT mobility of $0.21\text{ cm}^2\text{ V}^{-1}\text{ s}^{-1}$ and a clearly defined preferred conformation, as determined from theoretical calculations of the relation between rotational energy and dihedral angle, as well as atomic force microscopy (AFM) and X-ray diffraction (XRD) studies (7a). However, the mechanism of charge carrier transport in amorphous semiconductors remains poorly understood.

Here we report the synthesis, characterization, time-of-flight, and charge carrier mobility of a new soluble amorphous semiconducting polymer, poly(2,5-bis(3'-dodecyl-2,2'-bithiophen-5-yl)thieno[3,2-*b*]thiophene) (**NAP**). In addition, we determined the preferred conformation of **NAP** via a theoretical calculation, and on the basis of this finding suggest a possible route for charge transport in the amorphous film state. The polymer exhibited amorphous characteristics due to the improved flexibility imparted by the insertion of the unsubstituted thiophene between the rigid fused thiophene and dodecylthiophene in the main polymer backbone. The **NAP** TFT device exhibited a mobility of $0.02\text{ cm}^2\text{ V}^{-1}\text{ s}^{-1}$, the highest value ever reported for a TFT based on an amorphous semiconducting polymer.

RESULTS AND DISCUSSION

Synthesis and Thermal Properties. The synthesis of **NAP** is shown in Scheme 1. The monomer **2** was synthesized in 74% yield via a Grignard reaction of monomer **1** and 2-bromothiophene. The final monomer **3** was synthesized from **2** by a general bromination method using *N*-bromosuccinimide (NBS), and then purified by recrystallization using a methylene chloride/methanol solvent mixture. The other final monomer **4** was also synthesized according to an established method (3b). The synthesis of the polymer was carried out via microwave-assisted Stille cross-coupling in chlorobenzene. The crude polymer was purified by re-

precipitation and Soxhlet extraction with methanol and acetone to remove oligomeric materials. Its chemical structure was verified using ¹H NMR and elemental analysis. **NAP** was found to be moderately soluble in chloroform and highly soluble in chlorobenzene at room temperature. The number-average molecular weight (M_n) of **NAP** was found to be 13 800 (polydispersity index, PDI = 1.56) using gel permeation chromatography (GPC) with a polystyrene standard.

NAP was found to exhibit very good thermal stability, losing less than 5% of its weight on heating to about 420 °C, as determined using thermogravimetric analysis (TGA) under a nitrogen atmosphere. The thermal transitions of the polymer were studied using differential scanning calorimetry (DSC) under a nitrogen atmosphere (Figure 1). In contrast to the DSC patterns of semicrystalline polymer systems, the DSC thermogram for **NAP** did not show any peaks indicative of phase transitions from room temperature to 300 °C. This finding is consistent with **NAP** having an amorphous structure.

Optical Properties. The UV-vis absorption spectra of **NAP** in dilute chloroform solution and in a thin film state are shown in Figure 2. The thin film was spin-cast onto a quartz substrate and annealed at 100 °C for 30 min. The UV-vis absorption maximum appeared at 485 nm for **NAP**.

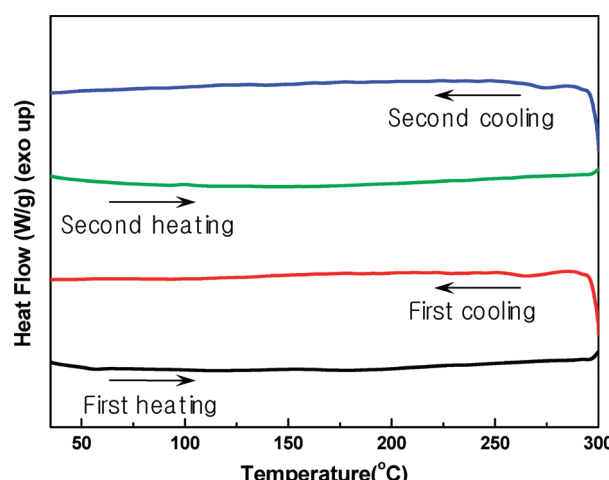


FIGURE 1. DSC thermograms of **NAP**.

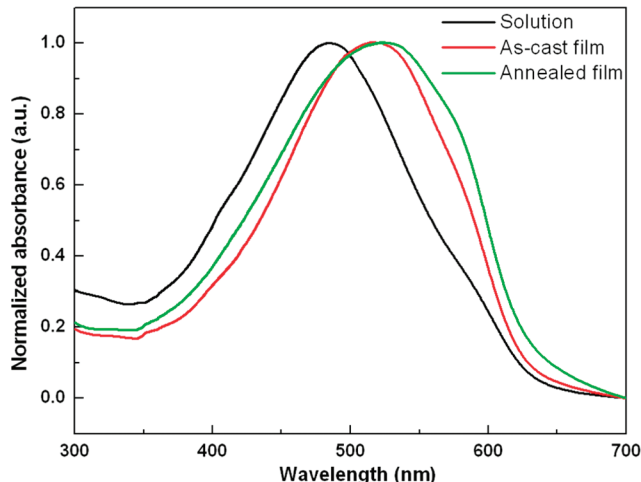


FIGURE 2. UV-vis absorption spectra of NAP in chloroform solution (black line), as-cast film (red line), and annealed film at 100 °C for 30 min (green line).

in dilute chloroform solution and at 520 nm for the thin film (annealed film: 523 nm). The red shift in the absorption on going from solution to thin film (or when the film was annealed) was much smaller than the shifts typically observed for semicrystalline polymers with interdigitated intermolecular ordering, such as PQT-12 (ca. 75 nm). In addition, no clear vibronic structures were evident in the UV-vis absorption spectra of NAP. These results indicate that NAP has similar conformations in the solution and solid states and can be attributed to weak stacking and weak electronic coupling caused by its highly disordered or amorphous intermolecular ordering between neighboring polymer chains (7).

X-ray Diffraction Results. X-ray diffraction (XRD) analyses of a NAP thin film were carried out to investigate the microstructural ordering. The thin film (thickness of 60 nm) was prepared by spin-casting from chloroform solvent onto octyltrichlorosilane (OTS)-modified Si/SiO₂ substrates followed by annealing at 100 °C for 30 min. The out-of-plane pattern did not show any reflection peaks, indicating that the sample had an amorphous structure, and the in-plane pattern showed a halolike broad peak at $2\theta = 21.0^\circ$, similar to regio-irregular P3HT (Figure 3). Annealing did not induce any change in the peak intensity or pattern. These results confirm that NAP films exhibit long-range amorphous states.

Film Morphologies. Figure 4 shows tapping-mode atomic force microscopy (AFM) images of NAP on OTS-modified silicon wafer substrates before and after annealing at 100 °C for 30 min. All NAP films, regardless of surface treatment (untreated, OTS- or octadecyltrichlorosilane (ODTS)-modified silicon substrates) or heat treatment, exhibited amorphous film states without any crystalline domains (see Figures S1 and S2 in the Supporting Information). In addition, all AFM images of NAP films showed very smooth and flat surface morphologies with a low root-mean-square (rms) surface roughness of 0.3–0.5 nm, indicative of amorphous film states.

Theoretical Calculations. Recent theoretical studies have indicated that polymer structures are affected by the

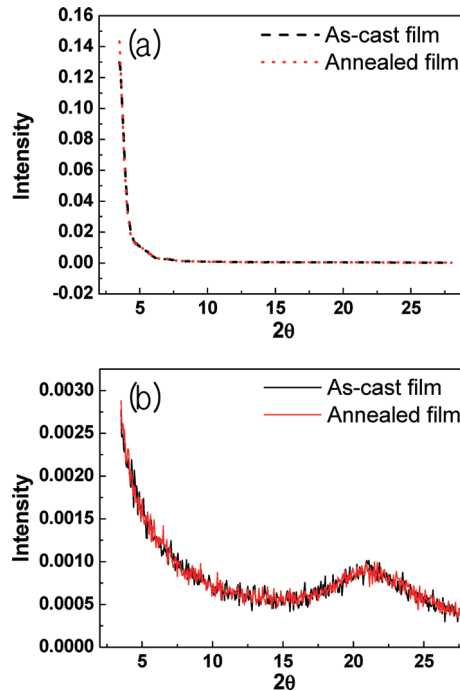


FIGURE 3. XRD patterns of NAP ((a) out-of-plane and (b) in-plane) thin films on OTS-treated SiO₂/Si substrate as-cast (black line) and after annealing at 100 °C for 30 min (red line).

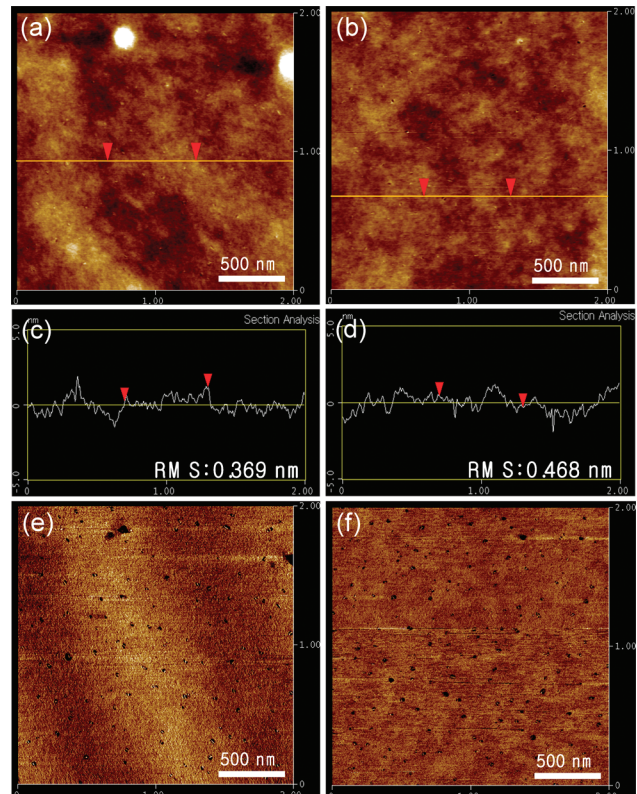


FIGURE 4. AFM images of NAP: (a, b) height images; (c, d) section analysis; (e,f) phase images of NAP thin films as-cast and annealed at 100 °C for 30 min, respectively, on OTS-modified SiO₂ substrates.

interaction between alkyl-thiophene moieties and fused aromatic rings (7a, 8). In an effort to rationalize substitution patterns of the rotational isomers of the NAP polymer, we performed quantum chemical calculations using the Gauss-

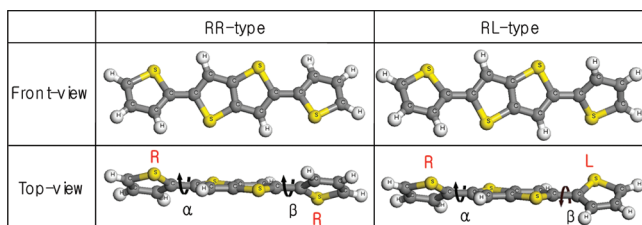


FIGURE 5. Front- and top-view of the considered NAP conformers (RR- and RL-forms).

ian 03 Program (9) by using the hybrid functional B3LYP (10) with the 6-31G* basis set. In **NAP**, both sides of the unsubstituted thiophenes next to the rigid fused thiophene ring are much more freely rotating than an alkyl-substituted thiophene directly attached to the fused ring, such as in PBTTT. As shown in Figure 5, **NAP** has two rotational conformers, the RR- and RL-forms. The two unsubstituted thiophenes of the RR-form are on opposite sides with respect to the fused core ring, whereas those of the RL-form are on the same side. By considering the energy as a function of the dihedral angles around two rotating bonds (α and β), we optimized the RR- and RL-conformers. Model compounds of **NAP** and PBTTT containing butylthiophenes instead of dodecylthiophenes, denoted mNAP and mPBTTT, respectively, were designed for the calculations and comparisons. The use of butyl chains in place of dodecyl chains gives a reasonable approximation of the molecular conformation while simplifying the calculations (8b). The optimized energy geometries of each model compound were obtained via a full geometry optimization

(see Figure S3 in the Supporting Information). To determine the probabilities of the RR- and RL-conformer states, we calculated the total energies of the optimized structures of the rotation conformers. For mNAP and mPBTTT, the RR-conformer was more stable than the RL-conformer by 0.03 and 1.82 kJ/mol, respectively (see Table S1 in the Supporting Information). Because the total energies of the two mNAP conformers were almost the same, the populations of the two conformers were almost equal at room temperature.

In addition, to understand the rotational barriers in mNAP and mPBTTT in more detail, relaxed potential energy surface (PES) scans as a function of dihedral angle α were calculated at 5° intervals with geometry optimizations. For mPBTTT, the calculated energy barrier between the two conformers was more than 3 kJ/mol (Figure 6a), confirming that mPBTTT prefers the RR-conformer over the RL-conformer because of the relatively high energy barrier between the two conformers. In contrast, the rotation of the mNAP model was relatively free because its PES energy maintained an almost constant value close to zero between 150° and -150° (Figure 6b). As a result, the RR- and RL-conformers are equally probable in the **NAP** polymer backbone chains from an energy standpoint. The existence of two conformers in itself may not have a significant impact on the intermolecular ordering, especially the $\pi-\pi$ stacking, of the polymer main backbone. However, the RL-form may be characterized by distortion of the alkyl-thiophenes next to the core unit containing both fused thiophene and unsubstituted

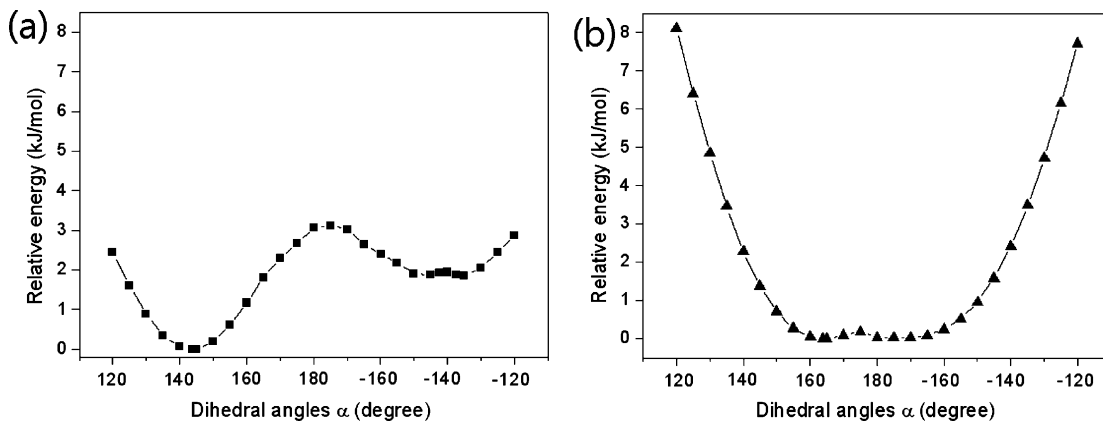


FIGURE 6. Relaxed PES scan of (a) mPBTTT and (b) mNAP. Relative total energies are plotted against the dihedral angle α .

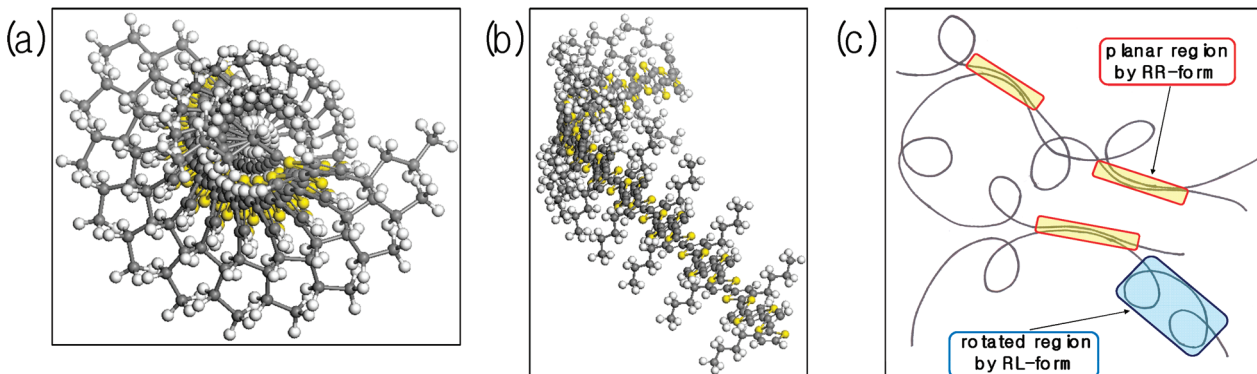


FIGURE 7. Modeled 12 units of (a) RL-form and (b) RR-form of mNAP and (c) schematic of amorphous polymer chains in a NAP film.

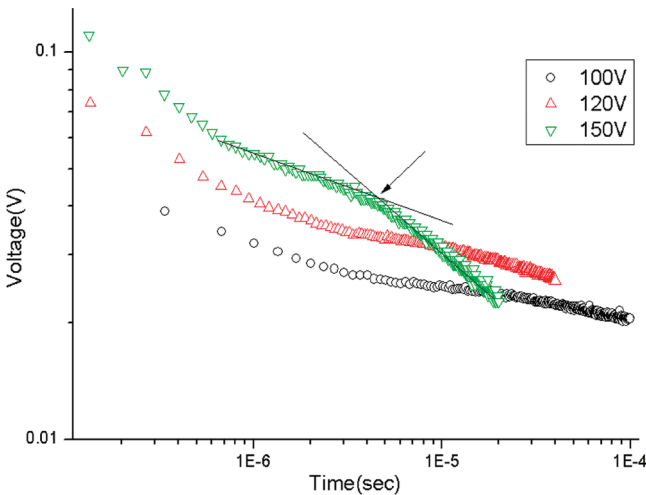


FIGURE 8. Time-of-flight photocurrent transients for NAP at room temperature for various applied voltages.

thiophenes. Such a distortion between the repeating units of the polymers might result in bending of the polymer main backbone.

The modeled 12 repeating units consisting exclusively of the RL-form of **NAP** exhibited a helical structure (Figure 7a). On the other hand, the system containing only the RR-form exhibited a relatively planar, slightly bent structure (Figure 7b). Although we cannot estimate the relative ratio of two conformers in the polymer backbone, we can infer from the energy analysis presented above that both conformations are likely to be present in the **NAP** polymer main backbone. Figure 7c shows a schematic representation of the amorphous structure that we predict the polymer chains will adopt in the film state. Relatively planar regions of the RR-form may result in $\pi-\pi$ stacking of the polymer main backbone, which can induce intermolecular charge transport. On the other hand, flexible regions of the RL-form mainly induce amorphous states of the polymer main backbone that can participate in intramolecular charge transport. As a result, in the bulk phase, **NAP** film may exhibit a long-range amorphous state capable of high charge carrier transport.

Time of Flight (TOF). We investigated charge transport in the amorphous **NAP** films under various electric fields using a conventional time-of-flight (TOF) technique. Thick drop-cast **NAP** films ($\sim 9 \mu\text{m}$) were prepared by pouring **NAP** solution (3 wt % in chloroform) onto an ITO prepatterned glass substrate and then vacuum-drying the sample at 80°C for 1 h. The thickness and flatness of the drop-cast **NAP** films were measured using an alpha-stepper. The penetration depth of the polymer films at 337 nm, the wavelength of the N_2 laser used in the TOF measurements, was less than $1 \mu\text{m}$, as determined by UV-vis spectroscopy. As the top electrode, a thin Al layer (20 nm) was deposited on the prepared **NAP** films to complete the devices. TOF experiments were performed in a vacuum cryogenic chamber. The TOF photocurrent transients were obtained by illuminating the samples with N_2 laser pulses of duration 6 ns and wavelength 337 nm under a dc bias. Figure 8 shows the current–voltage characteristics of the **NAP** film at various

Table 1. Performances of NAP-Based TFTs

surface treatment	mobility ($\text{cm}^2 \text{ V}^{-1} \text{ s}^{-1}$)		on/off ratio (as-spun/annealed)	threshold (V) (as-spun/annealed)
	as-spun	annealed		
none	2.0×10^{-3}	1.6×10^{-3}	$1 \times 10^4/1 \times 10^4$	$-1.5/-4.4$
OTS	4.0×10^{-3}	0.02	$1 \times 10^4/1 \times 10^5$	$-1.9/-2.0$
ODTS	5.2×10^{-3}	0.01	$1 \times 10^4/1 \times 10^4$	$-2.6/1.3$

bias voltages. The drift mobility of the **NAP** film was estimated from the slope of $\mu = d^2/Vt$, where d is the thickness of the film, V is the applied dc bias voltage, and t is the measured transit time. The drift hole mobility was found to be $3 \times 10^{-4} \text{ cm}^2 \text{ V}^{-1} \text{ s}^{-1}$ at a bias voltage of 150 V, which is similar to that of the well-known semiconducting polymer, P3HT (4). This result indicates that **NAP** is a good hole transport polymer despite having an amorphous structure in the film state.

TFT Characteristics. OTFTs based on **NAP** were fabricated using solution processing. Top-contact OTFTs were fabricated on the common gate of a highly n-doped silicon wafer with a 300 nm thick thermally grown SiO_2 dielectric layer. The surface of the substrate was modified with OTS or ODTD. Each organic semiconducting layer was spin-coated onto the substrate at 2000 rpm from a 0.5 wt % chloroform solution to a thickness of 60 nm. Gold source and drain electrodes (thickness 80 nm) were deposited on top of the thin film surface through a shadow mask. The channel length L was $100 \mu\text{m}$ and the channel width W was $2000 \mu\text{m}$. The OTFT characteristics were determined under ambient conditions without taking precautionary measures to protect the TFT devices from exposure to oxygen and moisture. The **NAP** OTFTs were found to exhibit typical p-channel TFT characteristics. The TFT mobilities were calculated in the saturation regime by using the following equation: (1) $I_D = (W/2L) \mu C_i (V_G - V_T)^2$, where I_D is the drain-source current in the saturated region, W and L are the channel width and length, respectively, μ is the field-effect mobility, C_i is the capacitance per unit area of the insulation layer, and V_G and V_T are the gate and threshold voltages, respectively.

The mobilities (calculated in the saturation regime), on/off ratios, and threshold voltages of the OTFTs are listed in Table 1. Without annealing, all **NAP**-based TFT devices showed similar values, ranging from 2.0×10^{-3} to $5.2 \times 10^{-3} \text{ cm}^2 \text{ V}^{-1} \text{ s}^{-1}$. After annealing, the TFT based on a **NAP** film on a bare silicon wafer showed only a slight change in TFT mobility, whereas the devices based on films on OTS- or ODTD-modified substrates exhibited small improvements in their TFT mobilities. This behavior, which can be attributed to the amorphous structure of the **NAP** films, stands in contrast to the behavior of TFT devices based on general semicrystalline thiophene-based polymers. In general, amorphous polymers have great advantages over polycrystalline films because the amorphous structure obviates the need for annealing and surface treatments. Figure 9 shows typical transfer and output curves of the OTFT device with **NAP** on an OTS-modified substrate as the semiconducting layer. The **NAP** TFT device exhibited a mobility of $0.02 \text{ cm}^2 \text{ V}^{-1} \text{ s}^{-1}$ with an on/off ratio of 1×10^5 and a very small threshold voltage

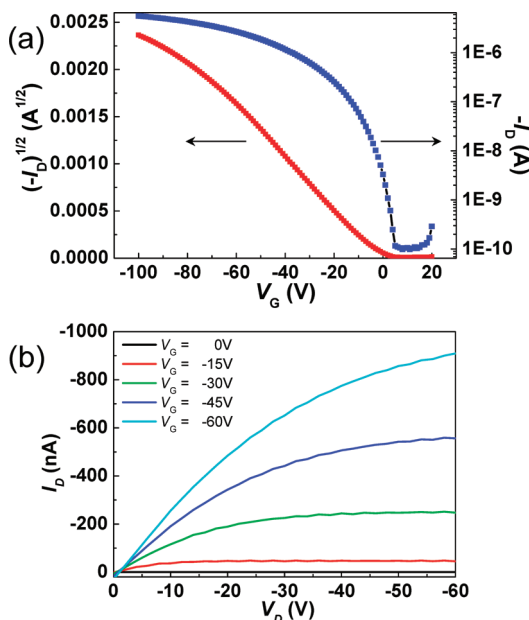


FIGURE 9. Current–voltage characteristics of NAP on an OTS-treated SiO_2 substrate. (a) Transfer curve at a constant source-drain voltage of -100 V . (b) Output curves at various gate voltages.

of -2.0 V that was insensitive to heat treatment. This mobility is the highest value reported to date for amorphous semiconducting polymers. In addition, very good saturation was observed in the output behaviors of the **NAP**-based TFTs and there was no noticeable contact resistance.

CONCLUSION

We successfully synthesized a new amorphous semiconducting polymer, **NAP**, via a microwave-assisted Stille coupling reaction. **NAP** exhibited amorphous characteristics, as determined by XRD, AFM, and computational calculations. In particular, the out-of-plane XRD pattern of **NAP** thin films clearly exhibited an amorphous microstructure both before and after annealing. In addition, AFM images of **NAP** films showed amorphous surface morphologies with low rms surface roughnesses of $0.3\text{--}0.5\text{ nm}$. Using computational calculations, we confirmed that **NAP** exhibits an amorphous structure, and suggested how an amorphous **NAP** semiconductor film can exhibit high carrier mobility. The **NAP**-based TFT device exhibited a mobility of $0.02\text{ cm}^2\text{ V}^{-1}\text{ s}^{-1}$ with an on/off ratio of 1×10^5 and a very small threshold voltage of -2.0 V . This mobility is the highest value ever reported for an amorphous semiconducting polymer. In addition, TFT devices based on **NAP** were only slightly affected by surface treatment (bare, OTS, or ODTs treatment) or heat treatment, in contrast to TFT devices based on semicrystalline polymer. Thus, **NAP** can be considered for use as a high-performance amorphous semiconductor.

EXPERIMENTAL SECTION

Measurements. The ^1H and ^{13}C NMR spectra were recorded using a Bruker AVANCE 400 spectrometer, with tetramethylsilane as an internal reference. Elemental analysis was performed using an EA 1110 Fisons analyzer. Mass spectra were collected on a MALDI TOF Voyager-DE STR. The number- and weight-average molecular weights of polymers were determined by gel

permeation chromatography (GPC) using a Viscotek T60A instrument with tetrahydrofuran (THF) as the eluent and polystyrene as standard. Differential scanning calorimetry (DSC) measurements were performed with a TA Q100 instrument and operated under a nitrogen atmosphere at a heating rate of $5\text{ }^\circ\text{C}/\text{min}$. UV-vis spectra were measured using a Jasco V-530 UV-vis spectrometer. An atomic force microscope (Multimode IIIa, Digital Instruments) operating in tapping-mode was used to image the surface morphologies of these semiconductors. Synchrotron X-ray diffraction analyses of the polymer films were performed at the 10C1 beamline (wavelength $\sim 1.54\text{ \AA}$) of the Pohang Accelerator Laboratory (PAL). The electrical characteristics of the TFTs were measured under ambient conditions with Keithley 2400 and 236 source/measure units. For all measurements, the channel length (L) was $100\text{ }\mu\text{m}$ and the channel width (W) was $2000\text{ }\mu\text{m}$. Field-effect mobilities were extracted in the saturation regime from the slope of the source-drain current.

Synthesis. 5,5'-Dibromo-4,4'-didodecyl-2,2'-bithiophene (1). The compound was synthesized according to the previously published procedure (3b). Yield: 2.73 g (86%). ^1H NMR (400 MHz , CDCl_3 , δ): 6.75 (s, 2H), 2.50 (t, 4H), 1.56 (m, 4H), 1.29 (m, 36H), 0.87 (t, 6H). ^{13}C NMR (100 MHz , CDCl_3 , δ): 142.9 , 136.2 , 124.4 , 107.9 , 31.9 , 29.67 , 29.64 , 29.61 , 29.5 , 29.4 , 29.3 , 29.2 , 22.7 , 14.1 . MS (MALDI-TOF) (m/z) 660 [M^+]. Anal. Calcd for $\text{C}_{32}\text{H}_{52}\text{Br}_2\text{S}_2$: C, 58.17 ; H, 7.93 ; S, 9.71 . Found: C, 58.56 ; H, 7.65 ; S, 9.86 .

5,5'-Dithiophene-4,4'-didodecyl-2,2'-bithiophene (2). A solution of 2-bromothiophene (2.37 g , 14.53 mmol) in 15 mL of anhydrous tetrahydrofuran (THF) was added dropwise to magnesium (0.47 g , 19.38 mmol) in anhydrous THF (10 mL), and the mixture was refluxed for 2 h at $60\text{ }^\circ\text{C}$ under nitrogen gas. The resulting mixture was added slowly to a solution of compound **1** (3.20 g , 4.84 mmol) and $\text{Pd}(\text{dpdf})\text{Cl}_2$ (0.08 g , 0.097 mmol) in anhydrous THF (25 mL) at $0\text{ }^\circ\text{C}$. The mixture was refluxed for 12 h at $60\text{ }^\circ\text{C}$, after which HCl solution (10%) was added. The mixture was washed with ethyl acetate, NaOH (10%), NaHCO_3 (1 M), and water. After being dried over anhydrous MgSO_4 , the solvent was evaporated. Purification on a silica column with $1:1$ hexane/ethylacetate as eluent, followed by recrystallization from dichloromethane/methanol gave compound **2**. Yield: 2.37 g (74%). ^1H NMR (CDCl_3 , 400 MHz , δ): 7.28 (d, 2H), 7.11 (d, 2H), 7.05 (t, 2H), 6.97 (s, 2H), 2.70 (t, 4H), 1.62 (m, 4H), 1.25 (m, 36H), 0.87 (t, 6H). ^{13}C NMR (CDCl_3 , 400 MHz , δ): 140.33 , 135.96 , 134.87 , 129.52 , 127.40 , 126.35 , 125.77 , 125.28 , 31.91 , 30.52 , 29.67 , 29.64 , 29.57 , 29.54 , 29.53 , 29.52 , 29.44 , 29.35 , 22.69 , 14.12 . MS (MALDI-TOF) 666 [M^+]. Anal. Calcd for $\text{C}_{40}\text{H}_{58}\text{S}_4$: C, 72.01 ; H, 8.76 ; S, 19.23 . Found: C, 72.15 ; H, 8.87 ; S, 18.98 .

5,5'-Dibromo(5,5'-dithiophene-4,4'-didodecyl-2,2'-bithiophene) (3). To a stirred solution of compound **2** (2.4 g , 3.59 mmol) in chloroform-acetic acid ($1:1$ v/v, 38 mL), *N*-bromosuccinimide (NBS) (1.31 g , 7.37 mmol) was added. The mixture was stirred at RT for 2 h , and then poured into water (100 mL) and extracted with ethyl acetate. The extract was successively washed with water, 5% sodium hydrogen carbonate aqueous solution, and brine. After being dried over anhydrous MgSO_4 , the solvent was evaporated. Purification on a silica column with $1:1$ hexane/ethylacetate as eluent, followed by recrystallization from dichloromethane/methanol gave compound **3** (a yellow solid). Yield: 2.10 g (71%). ^1H NMR (400 MHz , CDCl_3 , δ): 6.99 (d, 2H), 6.94 (s, 2H), 6.84 (d, 2H), 2.65 (t, 4H), 1.59 (m, 4H), 1.30 (m, 36H), 0.86 (t, 6H). MS (MALDI-TOF) (m/z) 824 [M^+]. Anal. Calcd for $\text{C}_{40}\text{H}_{56}\text{Br}_2\text{S}_4$: C, 58.24 ; H, 6.84 ; S, 15.55 . Found: C, 58.11 ; H, 6.76 ; S, 14.87 .

2,5-Bis(trimethylstannyly)thieno[3,2-b]thiophene (4). The compound was synthesized according to the previously published procedure (3b).

Poly(2,5-bis(*3*-dodecyl-2,2'-bithiophen-5-yl)thieno[3,2-*b*]thiophene) (NAP**).** A 50 mL flask was charged with a stirrer bar, compound **3** (1.01 g, 1.22 mmol), compound **4** (0.57 g, 1.22 mmol), tris(dibenzylideneacetone)dipalladium (0) (0.023 g, 0.025 mmol), tri(*o*-tolyl)phosphine (0.030 g, 0.098 mmol), and chlorobenzene (12 mL). The flask was placed into a microwave reactor and heated to 200 °C. The mixture was heated with stirring at 160 °C for 120 s, 180 °C for 120 s, and finally, 200 °C for 12 min. The reaction mixture was cooled to about 50 °C, and then slowly added to a vigorously stirred mixture of 230 mL of methanol and 13 mL of 1 N aqueous HCl. The polymer fibers were collected by filtration and reprecipitation from methanol and acetone. The polymer was purified further by washing for 2 days in a Soxhlet apparatus with methanol, acetone to remove oligomers and catalyst residues, and by column chromatography with a chloroform solution of the polymer. The reprecipitation procedure in chloroform/methanol was then repeated several times. The final product, a red polymer, was obtained after drying in vacuo at 60 °C. ¹H NMR (400 MHz, CDCl₃, δ): aromatic; 7.28 (2H) 7.11 (2H), 7.05 (2H), 6.98 (2H), aliphatic; 2.72 (4H), 1.66 (4H), 1.38 (36H), 0.86 (6H); Anal. Calcd for C₄₆H₆₀S₆: C, 68.60; H, 7.51; S, 23.89. Found: C, 68.74; H, 7.69; S, 23.16.

Acknowledgment. This research was supported by a grant (F0004011-2009-32) from the Information Display R&D Center, one of the Knowledge Economy Frontier R&D Program funded by the Ministry of Knowledge Economy of Korean Government.

Supporting Information Available: AFM images (on bare and ODTs-modified SiO₂ substrates); calculated optimized structures, dihedral angles, and relative total energy; transfer characteristics of **NAP** thin films (PDF). This material is available free of charge via the Internet at <http://pubs.acs.org>.

REFERENCES AND NOTES

- (1) (a) Dimitrakopoulos, C. D.; Mascaro, D. *J. Adv. Mater.* **2002**, *14*, 99. (b) Sirringhaus, H.; Brown, P. J.; Friend, R. H.; Nielsen, M. M.; Bechgaard, K.; Langeveld-Voss, B. M. W.; Spiering, A. J. H.; Janssen, R. A. J.; Meijer, E. W.; Herwig, P.; de Leeuw, D. M. *Nature* **1999**, *401*, 685. (c) Bao, Z. *Adv. Mater.* **2000**, *12*, 227. (d) Li, W.; Katz, H. E.; Lovinger, A. J.; Laquindanum, J. G. *Chem. Mater.* **1999**, *11*, 458. (e) Forrest, S. R. *Nature* **2004**, *428*, 911. (f) Katz, H. E.; Bao, Z.; Gilat, S. L. *Acc. Chem. Res.* **2001**, *34*, 359. (g) Bendikov, M.; Wudl, F.; Perepichka, D. F. *Chem. Rev.* **2001**, *111*, 1069. (h) Zhang, M.; Tsao, H. N.; Pisula, W.; Yang, C.; Mishra, A. K.; Mullen, K. *J. Am. Chem. Soc.* **2007**, *129*, 3472. (i) Usta, H.; Lu, G.; Facchetti, A.; Marks, T. J. *J. Am. Chem. Soc.* **2006**, *128*, 9034. (j) Allard, S.; Forster, M.; Souharce, B.; Thiem, H.; Scherf, U. *Angew. Chem., Int. Ed.* **2008**, *47*, 4070. (k) Sirringhaus, H. *Adv. Mater.* **2005**, *17*, 2411.
- (2) Ong, B. S.; Wu, Y.; Liu, P.; Gardner, S. *Adv. Mater.* **2005**, *17*, 1141.
- (3) (a) Ong, B. S.; Wu, Y.; Liu, P.; Gardner, S. *J. Am. Chem. Soc.* **2004**, *126*, 3378. (b) McCulloch, I.; Heeney, M.; Bailey, C.; Genevicius, K.; Macronald, I.; Shkunov, M.; Sparrowe, D.; Tierney, S.; Wagner, R.; Zhang, W.; Chabiny, M. L.; Kline, R. J.; McGehee, M. D.; Toney, M. F. *Nat. Mater.* **2006**, *5*, 328.
- (4) Chung, D. S.; Lee, S. J.; Park, J. W.; Choi, D. B.; Lee, D. H.; Park, J. W.; Shin, S. C.; Kim, Y.-H.; Kwon, S.-K.; Park, C. E. *Chem. Mater.* **2008**, *20*, 3450.
- (5) Kong, H.; Lee, D. H.; Kang, I.-N.; Lim, E.; Jung, Y. K.; Park, J.-H.; Ahn, T.; Yi, M. H.; Park, C. E.; Shim, H.-K. *J. Mater. Chem.* **2008**, *18*, 1895.
- (6) (a) Veres, J.; Ogier, S. D.; Leeming, S. W.; Cupertino, D. C.; Khaffaf, S. M. *Adv. Funct. Mater.* **2003**, *13*, 199. (b) Veres, J.; Ogier, S.; Lloyd, G.; Leeuw, D. D. *Chem. Mater.* **2004**, *16*, 4543.
- (7) (a) Liu, J.; Zhang, R.; Sauvé, G.; Kowalewski, T.; McCullough, R. D. *J. Am. Chem. Soc.* **2008**, *130*, 13167. (b) Schmidt, R.; Göttling, S.; Leusser, D.; Stalke, D.; Krause, A.-M.; Würthner, F. *J. Mater. Chem.* **2006**, *16*, 3708.
- (8) (a) Zhang, X.; Köhler, M.; Matzger, A. J. *Macromolecules* **2004**, *37*, 6306. (b) Miguel, L. S.; Matzger, A. J. *Macromolecules* **2007**, *40*, 9233. (c) Surin, M.; Sonar, P.; Grimsdale, A. C.; Müllen, K.; Lazzaroni, R.; Leclère, P. *Adv. Funct. Mater.* **2005**, *15*, 1426.
- (9) Frisch, M. J. Trucks, G. W.; Schlegel, H. B.; Scuseria, G. E.; Robb, M. A.; Cheeseman, J. R.; Montgomery, J. A., Jr.; Vreven, T.; Kudin, K. N.; Burant, J. C.; Millam, J. M.; Iyengar, S. S.; Tomasi, J.; Barone, V.; Mennucci, B.; Cossi, M.; Scalmani, G.; Rega, N.; Petersson, G. A.; Nakatsuji, H.; Hada, M.; Ehara, M.; Toyota, K.; Fukuda, R.; Hasegawa, J.; Ishida, M.; Nakajima, T.; Honda, Y.; Kitao, O.; Nakai, H.; Klene, M.; Li, X.; Knox, J. E.; Hratchian, H. P.; Cross, J. B.; Bakken, V.; Adamo, C.; Jaramillo, J.; Gomperts, R.; Stratmann, R. E.; Yazyev, O.; Austin, A. J.; Cammi, R.; Pomelli, C.; Ochterski, J. W.; Ayala, P. Y.; Morokuma, K.; Voth, G. A.; Salvador, P.; Dannenberg, J. J.; Zakrzewski, V. G.; Dapprich, S.; Daniels, A. D.; Strain, M. C.; Farkas, O.; Malick, D. K.; Rabuck, A. D.; Raghavachari, K.; Foresman, J. B.; Ortiz, J. V.; Cui, Q.; Baboul, A. G.; Clifford, S.; Cioslowski, J.; Stefanov, B. B.; Liu, G.; Liashenko, A.; Piskorz, P.; Komaromi, I.; Martin, R. L.; Fox, D. J.; Keith, T.; Al-Laham, M. A.; Peng, C. Y.; Nanayakkara, A.; Challacombe, M.; Gill, P. M. W.; Johnson, B.; Chen, W.; Wong, M. W.; Gonzalez, C.; Pople, J. A. *Gaussian 03, Revision C.02*; Gaussian, Inc.: Wallingford, CT, 2004.
- (10) (a) Becke, A. D. *J. Chem. Phys.* **1993**, *98*, 5648. (b) Perdew, J. P. *Phys. Rev. B* **1986**, *33*, 8822.

AM9008852